Frontiers in Bioscience Landmark

Front. Biosci. (Landmark Ed) **2025**; 30(11): 47322
https://doi.org/10.31083/FBL47322

Original Research

Proteomic Characterization of Necroptosis-Related Proteins Reveals the Role of Endometrial Dysfunction in Predicting Pregnancy Outcomes in Polycystic Ovary Syndrome

Wenhu Xin[1,†], Kexin Wang[1,†], Chengbin Tao[1], Xiuli Tian[1], Fang Wang[1,*]

[1]Country Reproductive Medicine Center, The Second Hospital of Lanzhou University, 730030 Lanzhou, Gansu, China
*Correspondence: ery_fwang@lzu.edu.cn (Fang Wang)
[†]These authors contributed equally.

Academic Editor: Sung Eun Kim
Submitted: 13 October 2025 Revised: 14 November 2025 Accepted: 19 November 2025 Published: 27 November 2025

Abstract

Objective: This study investigated necroptosis-related molecular alterations in the endometrium of patients with polycystic ovary syndrome (PCOS) using quantitative proteomic analysis and developed a predictive model for pregnancy outcomes based on these findings. **Methods**: Liquid chromatography-tandem mass spectrometry was used to identify and quantify endometrial proteins. Differentially expressed proteins (DEPs) were screened and subjected to Gene Ontology and Kyoto Encyclopedia of Genes and Genomes (KEGG) enrichment analyses to identify key pathways. Candidate prognostic necroptosis–related proteins were obtained by intersecting DEPs with the necroptosis gene set, followed by univariate Cox and Least Absolute Shrinkage and Selection Operator (LASSO) regression analyses to select those associated with pregnancy outcomes and construct a predictive model. **Results**: A total of 611 DEPs were identified (132 upregulated and 479 downregulated). KEGG enrichment revealed significant involvement of the necroptosis pathway. Six necroptosis-related proteins were identified using Cox and LASSO regression analyses and used to construct the predictive model. Kaplan–Meier analysis showed that the low-risk group had significantly better pregnancy outcomes than the high-risk group. The model achieved an area under the receiver operating characteristic curve of 0.903 for predicting live birth at 37 weeks, and decision curve analysis demonstrated superior clinical benefit compared to conventional clinical indicators. Furthermore, correlation analysis revealed significant associations between necroptosis-related proteins and classical endometrial receptivity markers, suggesting potential molecular crosstalk. **Conclusion**: Proteomic profiling revealed enrichment of the necroptosis pathway in the endometrium of patients with PCOS. The constructed model indicated preliminary predictive potential for pregnancy outcomes, suggesting that necroptosis may contribute to impaired endometrial receptivity.

Keywords: necroptosis; polycystic ovary syndrome; endometrial receptivity; proteomics; pregnancy outcome; predictive model

1. Introduction

Polycystic ovary syndrome (PCOS) is one of the most common endocrine disorders among women of reproductive age, affecting approximately 10% of the female population [1]. The pathogenesis of PCOS is multifactorial and involves ovulatory dysfunction, hyperandrogenism, and insulin resistance (IR) [2,3]. Recent evidence suggests that beyond ovarian factors, local metabolic disturbances and inflammatory microenvironmental changes in the endometrium play pivotal roles in implantation failure [4]. During assisted reproductive treatment, women with PCOS often exhibit decreased endometrial receptivity; even when high-quality embryos are obtained, their pregnancy outcomes remain significantly poorer than those in women without PCOS [5–7]. Hyperandrogenism and IR synergistically disrupt glucose–lipid metabolism, oxidative balance, and immune–inflammatory homeostasis within the endometrium, leading to impaired decidualization, aberrant angiogenesis, and defective embryo implantation [8–11]. Moreover, recent studies indicate that hyperandrogenism, IR, and obesity are associated with downregulated expression of endometrial receptivity markers and elevated inflammatory cytokines, which may further compromise implantation and gestational success [8]. However, the molecular mechanisms underlying endometrial impairment in PCOS remain incompletely understood, necessitating further investigation into the roles of cell death and inflammatory responses in its pathophysiology.

Necroptosis, a form of regulated inflammatory cell death mediated primarily by receptor-interacting protein kinase 1, receptor-interacting protein kinase 3, and mixed lineage kinase domain-like, triggers immune activation and promotes chronic inflammation within the endometrial microenvironment [12–14]. Increasing evidence indicates that excessive necroptosis contributes to ovarian dysfunction by disrupting granulosa cell survival and steroidogenesis, aggravating follicular atresia and ovulatory failure [15]. In the endometrium, necroptosis-associated signaling amplifies cytokine release and immune cell infiltration, leading to local inflammatory remodeling and impaired receptivity [16]. Furthermore, dysregulated necroptosis interferes with

embryo–endometrium communication, resulting in implantation failure and early pregnancy loss [17]. However, its precise role in PCOS-related endometrial dysfunction and pregnancy outcomes remains poorly understood, necessitating further research into the underlying mechanisms.

In this study, we performed proteomic and clinical data analyses on endometrial samples from patients with PCOS to explore the relationship between necroptosis-related proteins and PCOS-associated endometrial dysfunction, as well as their impact on pregnancy outcomes. By constructing a predictive model, we established a necroptosis–pregnancy outcome association framework, providing a theoretical basis for developing targeted strategies to improve reproductive prognosis in patients with PCOS.

2. Materials and Methods

2.1 Study Population and Sample Collection

This study included women treated at the Reproductive Medicine Center of the Second Hospital of Lanzhou University between May 2024 and May 2025. A total of 36 endometrial samples were collected, including 30 from patients diagnosed with PCOS undergoing *in vitro* fertilization–embryo transfer and 6 from healthy fertile controls.

Given the exploratory nature of this proteomic study, no *a priori* power calculation was performed. A post hoc power analysis based on the observed average effect size across six key differentially expressed proteins (Cohen's d = 1.42; $n_1 = 30$, $n_2 = 6$; $\alpha = 0.05$, two-tailed) indicated a statistical power of approximately 0.95, suggesting adequate sensitivity to detect large intergroup differences.

PCOS was diagnosed according to the Rotterdam criteria, requiring at least two of the following: (1) oligo- or anovulation; (2) clinical or biochemical hyperandrogenism; and (3) polycystic ovarian morphology ($\geq$12 follicles or ovarian volume $>$10 mL). Inclusion criteria were women aged 21–40 years with infertility lasting $\geq$1 year and partners with normal semen parameters. Exclusion criteria included tubal obstruction, endometriosis, uterine malformation or adhesions, diabetes, thyroid dysfunction, hepatic or renal impairment, and recent (within 3 months) use of medications affecting hormonal or metabolic function (e.g., contraceptives, insulin sensitizers, corticosteroids). Healthy controls were women with spontaneous conception and normal early pregnancy who had no history of metabolic or chronic inflammatory diseases and had never received assisted reproductive therapy.

All participants underwent endometrial biopsy under hysteroscopy during the midluteal phase. Biopsy samples were rinsed in saline, snap-frozen in liquid nitrogen, and stored at –80 °C for proteomic analysis.

This study was approved by the Ethics Committee of the Second Hospital of Lanzhou University (Approval No. 2025A-774). Written informed consent was obtained from all participants. All procedures were conducted in accordance with the ethical principles of the Declaration of Helsinki.

2.2 Clinical Data Collection and Pregnancy Outcome Definition

Baseline clinical data included maternal age, height, weight, and body mass index (BMI). In addition, age and BMI were further categorized into clinically relevant subgroups ($<$25, 26–30, $>$30 years; $<$18.5, 18.5–24.9, $\geq$25 kg/m^2) for descriptive comparison between groups [18,19].

Venous blood was collected on the day of endometrial biopsy for biochemical and hormonal measurements. All biochemical and hormonal data were obtained from the hospital's electronic medical record system, with assays performed by the Department of Clinical Laboratory under standardized procedures. Serum levels of anti-Müllerian hormone (AMH), luteinizing hormone (LH), follicle-stimulating hormone (FSH), testosterone (T), and fasting insulin (FINS) were measured using a chemiluminescence immunoassay on the Cobas 8000 analyzer (E602; Roche Diagnostics, Basel, Switzerland). Fasting blood glucose (FBG) and lipid parameters including total cholesterol (TC) and triglycerides (TGs) were measured enzymatically on the Cobas 8000 analyzer (C702; Roche Diagnostics). The homeostatic model assessment of IR (HOMA-IR) was calculated as follows: HOMA-IR = [FBG (mmol/L) $\times$ FINS (μU/mL)] / 22.5 [20,21].

Clinical pregnancy was confirmed by both ultrasonography and laboratory testing. Specific criteria included observation of an intrauterine gestational sac and fetal cardiac activity via transvaginal ultrasound at $\geq$5 weeks. Pregnancy outcomes were categorized as live birth or adverse pregnancy. Adverse pregnancy outcomes included: biochemical pregnancy (defined as transient elevation of serum beta human chorionic gonadotropin without ultrasound evidence of a gestational sac), early miscarriage (defined as spontaneous pregnancy loss before 12 weeks of gestation), and late miscarriage (defined as fetal loss between 12 and 24 weeks of gestation). Pregnancy duration was recorded from the time of embryo transfer to final outcome for use in survival analyses and model construction.

2.3 Protein Extraction, Digestion, and Quantification

Endometrial tissues were homogenized (FastPrep-24 5G; MP Biomedicals, Santa Ana, CA, USA) under liquid nitrogen and lysed in SDT lysis buffer (4% Sodium dodecyl sulfate (SDS), 100 mM dithiothreitol (DTT), 150 mM Tris-HCl, pH 8.0) (ED-8452; Guangzhou Saiguo Biotechnology, Guangzhou, China). Samples were shaken at 6.0 m/s for 60 s, followed by six cycles of intermittent sonication (5 s on, 5 s off). Lysates were heated at 100 °C for 15 min and centrifuged at 14,000 g for 40 min. Supernatants were collected for quantification using the BCA assay (G2026; Wuhan Servicebio, Hubei, China).

Proteins were alkylated with 100 mM iodoacetamide for 30 min in the dark and filtered using 10 kDa ultrafiltration units. After washing with urea-alkylating (UA) buffer and 25 mM NH_4HCO_3, proteins were digested overnight with trypsin (1:50, w/w) at 37 °C. Peptides were desalted using C18 cartridges (567270U; Sigma, St. Louis, MO, USA), vacuum dried, and reconstituted in 0.1% formic acid. The peptide concentration was measured at 280 nm, after which samples were fractionated into 10 fractions using a high pH reversed-phase kit (84868; Thermo Fisher Scientific, Waltham, MA, USA) and then stored in 0.1% formic acid.

2.4 LC–MS/MS Analysis and Data Processing

Peptide fractions were analyzed by Shanghai Applied Protein Technology Co., Ltd. (Shanghai, China) using the Evosep One LC system coupled to a timsTOF Pro mass spectrometer (Bruker, Billerica, MA, USA).

Data-dependent acquisition (DDA) was used to generate a spectral library, followed by data-independent acquisition (DIA) for quantification. DDA settings were as follows: precursor scan range 300–1800 m/z; resolution 60,000; automatic gain control (AGC) target 3×10^6; max injection time (IT) 25 ms; and dynamic exclusion 30 s. Each full MS1 scan was followed by 20 MS2 scans (resolution 15,000, AGC target 5×10^6, normalized collision energy 30 eV). DIA acquisition used a full scan range of 300–1800 m/z with MS1 resolution of 120,000, AGC target of 3×10^6, and maximum IT of 50 ms. The LC gradient was 90 min at a flow rate of 250 nL/min, using 0.1% formic acid in 80% acetonitrile as mobile phase B. Quality control samples—pooled from all samples—were analyzed after every six runs to ensure data stability.

Raw MS data were processed with Spectronaut (version 14.4.200727.47784; Biognosys AG, Schlieren, Switzerland) using the UniProt human protein database. Search parameters were as follows: trypsin digestion (maximum of 2 missed cleavages); one fixed modification (carbamidomethylation); and two variable modifications (oxidation on methionine residues and acetylation on the protein's N-terminus. Precursor and fragment tolerances were 10 ppm and 0.02 Da, respectively, with a false discovery rate (FDR) $<1\%$, calculated as FDR = N(decoy) $\times$ 2 / [N(decoy) + N(target)], ensuring a 99% confidence level for all reported identifications. DIA data were $\log_2$-transformed and normalized; proteins with $>50\%$ missing values were excluded. Differential expression was determined by the Student's *t*-test with Benjamini–Hochberg correction (fold change >1.5, FDR <0.05).

2.5 Identification and Functional Enrichment of DEPs

DEPs were identified using the "limma" package (version 3.66.0; Bioconductor, https://bioconductor.org/packages/limma/) in R (v4.5.1; R Foundation for Statistical Computing, Vienna, Austria) with thresholds $|\log_2 FC| > 0.58$ and FDR <0.05. Subcellular localization was predicted using CELLO v2.5. Gene Ontology (GO) and Kyoto Encyclopedia of Genes and Genomes (KEGG) enrichment analyses were conducted using the "clusterProfiler" package (version 4.18.2; Bioconductor, https://bioconductor.org/packages/clusterProfiler/) to elucidate potential biological processes, cellular components, molecular functions, and pathways.

2.6 Analysis of Necroptosis-Related DEPs

Necroptosis-related gene sets were retrieved from GeneCards (https://www.genecards.org/), KEGG (https://www.kegg.jp/), and National Center for Biotechnology Information (NCBI) (https://www.ncbi.nlm.nih.gov/) databases. These genes were intersected with the DEPs to identify necroptosis-related DEPs. Machine learning algorithms were applied using R packages "e1071", "kernlab", and "caret" to screen for core necroptosis-associated proteins.

Protein–protein interaction (PPI) networks were constructed using the STRING database (v11.5, https://string-db.org/) and visualized in Cytoscape. Correlation networks among necroptosis proteins were plotted using "corrplot", "reshape2", and "igraph".

2.7 Construction and Validation of the Risk Model

Univariate Cox regression (R package "survival") was used to identify necroptosis-related DEPs significantly associated with pregnancy outcomes ($p < 0.05$). Then the Least Absolute Shrinkage and Selection Operator (LASSO)–Cox regression (R package "glmnet", seed = 2000) was applied as a penalized method to minimize overfitting, with internal 10-fold cross-validation to enhance model stability. The necroptosis risk (NecroSig) score was calculated as: NecroSig Score = $\sum_{i=1}^{n} \beta i \times Expri$, where β_1–β_n are LASSO coefficients and $Expr_1$–$Expr_n$ are standardized expression values [$\log_2$(TPM + 1)].

Patients were divided into high- and low-risk groups based on the median risk score. Principal component analysis was conducted using "Rtsne" and "ggplot2". Kaplan–Meier survival analysis was performed to compare pregnancy outcomes between groups. Time-dependent receiver operating characteristic (ROC) curves ("timeROC") were used to assess predictive accuracy at 6, 28, and 37 weeks of gestation. Decision curve analysis (DCA) ("ggDCA") compared the net clinical benefit of the NecroSig model with conventional predictors (age, BMI, HOMA-IR, lipids). A nomogram and calibration curve were generated to evaluate consistency between predicted and observed live birth rates.

2.8 Statistical Analyses

All statistical analyses were performed using SPSS 26.0 (IBM Corp., Armonk, NY, USA) and R 4.5.1. Normality was tested with the Kolmogorov–Smirnov test. Continu-

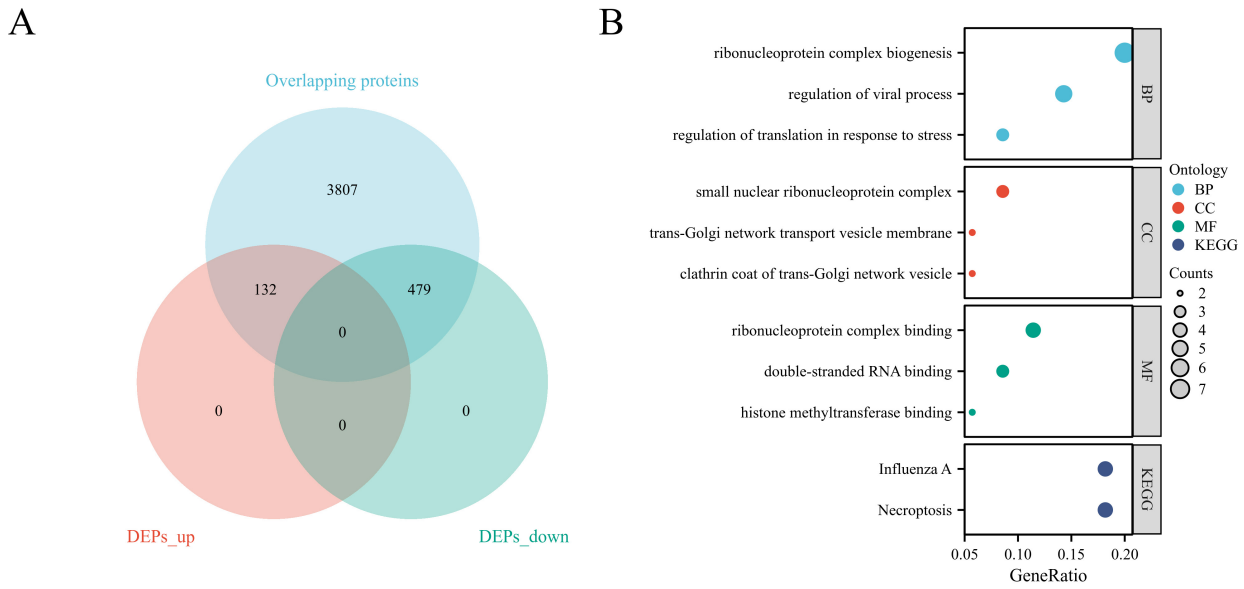

Fig. 1. Identification and enrichment analysis of differentially expressed proteins. (A) Volcano plot showing DEPs between PCOS and control endometria. (B) Functional enrichment analysis of DEPs. DEPs, differentially expressed proteins; KEGG, Kyoto Encyclopedia of Genes and Genomes; BP, Biological Process; CC, Cellular Component; MF, Molecular Function.

ous variables with non-normal distribution are expressed as the median (P25, P75) and were compared using the Mann–Whitney U test; categorical variables were compared using the chi-square or Fisher's exact test. $p < 0.05$ was considered statistically significant. Spearman's rank correlation analysis was performed to evaluate the associations of necroptosis-related proteins with both clinical metabolic indicators and endometrial receptivity markers within the PCOS cohort. Correlations with $p < 0.05$ were considered statistically significant. Missing values for clinical and proteomic variables were examined prior to analysis. Proteins with >50% missing values were excluded, and remaining missing data were handled using pairwise deletion for correlation analysis and complete-case analysis for regression models. The proportional hazards assumption of the Cox regression model was verified using Schoenfeld residuals, and no significant violation was detected ($p > 0.05$).

3. Results

3.1 Clinical Characteristics and Pregnancy Outcomes

The clinical and pregnancy data of the two groups are summarized in Table 1. Women with PCOS showed significant elevations in FINS, HOMA-IR, AMH, LH, LH/FSH ratio, and T levels, along with a marked decrease in endometrial thickness (ET). No significant differences were observed in age, height, weight, BMI, FSH, or gestational duration of live birth between the two groups. In the control group, no adverse pregnancy outcomes were observed. By contrast, among the 30 women with PCOS, 14 experienced adverse pregnancy outcomes including 10 early miscarriages, 3 biochemical pregnancies, and 1 late miscarriage. No cases of preterm delivery or stillbirth were recorded.

3.2 Proteomic Profiling and Identification of DEPs

Quantitative proteomic analysis of all endometrial samples was performed to identify PCOS-associated proteins. A total of 4425 proteins were commonly detected in both PCOS and control samples. Among them, 611 proteins were identified as differentially expressed, including 132 upregulated and 479 downregulated proteins in the PCOS group (Fig. 1A).

3.3 Functional Enrichment Analysis of DEPs

To further elucidate the biological functions of the DEPs, GO and KEGG pathway enrichment analyses were performed (Fig. 1B). GO analysis revealed that the DEPs were significantly enriched in biological processes such as ribonucleoprotein complex biogenesis, regulation of viral process, and translational control in response to stress. For the cellular component category, DEPs were mainly associated with the small nuclear ribonucleoprotein complex, trans-Golgi network transport vesicle membrane, and clathrin-coated vesicle. Regarding molecular function, enrichment was observed in double-stranded RNA binding, histone methyltransferase binding, and ribonucleoprotein complex binding. KEGG pathway analysis identified influenza A infection and necroptosis as the two most significantly enriched pathways, indicating a potential inflammatory association underlying endometrial dysfunction in PCOS, rather than confirming a direct causal mechanism.

3.4 Identification of Prognostic Necroptosis-Related Proteins

To determine necroptosis-related DEPs associated with PCOS prognosis, 628 necroptosis-related genes were

Table 1. Clinical characteristics and pregnancy outcomes of women in the PCOS and control groups.

	Control group (n = 6)	PCOS group (n = 30)	*p*
Age (years)	26.83 ± 3.19	25.67 ± 3.09	0.406
≤25 years (%)	33.3 (2/6)	46.7 (14/30)	
26–30 years (%)	50.0 (3/6)	40.0 (12/30)	
>30 years (%)	16.7 (1/6)	13.3 (4/30)	
Height (cm)	163.17 ± 5.12	160.87 ± 4.91	0.345
Weight (kg)	60.42 ± 6.41	62.27 ± 10.74	0.688
BMI (kg/m^2)	21.80 ± 2.84	24.02 ± 3.75	0.181
<18.5 kg/m^2 (%)	16.7 (1/6)	6.7 (2/30)	
18.5–24.9 kg/m^2 (%)	66.6 (4/6)	50.0 (15/30)	
≥25 kg/m^2 (%)	16.7 (1/6)	43.3 (13/30)	
AMH (ng/mL)	1.71 ± 1.14	9.39 ± 3.94	<0.001*
LH (IU/L)	5.19 ± 0.52	11.99 ± 4.37	<0.001*
FSH (IU/L)	5.35 (5.10, 6.57)	7.28 (6.36, 7.96)	0.018*
LH/FSH	0.91 ± 0.07	1.76 ± 0.67	<0.001*
T (ng/mL)	25.74 ± 12.06	42.53 ± 18.29	0.039*
FINS (mIU/L)	7.32 (5.75, 12.18)	16.00 (9.76, 26.03)	0.010*
HOMA-IR	1.73 ± 0.85	4.55 ± 3.19	0.041*
ET (mm)	9.79 ± 0.80	4.09 ± 1.45	<0.001*
Gestational duration			
Live birth time (weeks)	37.83 ± 1.04	38.47 ± 1.59	0.374
Gestational time at adverse pregnancy (weeks)	-	7.93 ± 8.64	-
Rate of adverse pregnancy outcomes (%)	0 (0/6)	46.7 (14/30)	
Early miscarriages (%)	-	71.4 (10/14)	
Late miscarriage (%)	-	7.1 (1/14)	
Biochemical pregnancies (%)	-	21.4 (3/14)	

Notes: * Statistically significant difference between groups ($p < 0.05$). PCOS, polycystic ovary syndrome; BMI, body mass index; AMH, anti-Müllerian hormone; LH, luteinizing hormone; FSH, follicle-stimulating hormone; T, testosterone; FINS, fasting insulin; HOMA-IR, homeostatic model assessment of IR; ET, endometrial thickness.

retrieved from public databases (GeneCards, KEGG, and NCBI) and intersected with the PCOS DEPs, yielding 15 overlapping proteins.

Univariate Cox regression identified several necroptosis-related proteins significantly associated with pregnancy outcomes. Subsequent LASSO regression further reduced the candidates to six prognostically relevant necroptosis-related proteins: dynamin 1 like (DNM1L), thioredoxin (TXN), eukaryotic translation initiation factor 2 alpha kinase 2 (EIF2AK2), adenosine deaminase acting on RNA (ADAR), calmodulin-dependent protein kinase II gamma (CAMK2G), and calmodulin-dependent protein kinase II delta (CAMK2D) (Fig. 2A–C).

A PPI network constructed using the STRING database illustrated their putative molecular interconnections (Fig. 2D), whereas the correlation heatmap demonstrated their expression relationships (Fig. 2E).

3.5 Construction and Evaluation of the NecroSig Prognostic Model

Using the six prognostic necroptosis-related proteins, a necroptosis risk model (NecroSig) was established based on 30 patients with PCOS with pregnancy outcome data. The risk score was calculated as follows:

$$\text{NecroSig (PCOS)} = 0.000280179 \times \text{DNM1L} - 0.000601845 \times \text{TXN} + 0.003339755 \times \text{EIF2AK2} + 0.004178775 \times \text{ADAR} - 0.001023549 \times \text{CAMK2G} - 0.000960423 \times \text{CAMK2D}$$

Among these, DNM1L, EIF2AK2, and ADAR had positive coefficients, indicating potential risk factors for adverse pregnancy outcomes; whereas TXN, CAMK2G, and CAMK2D showed negative coefficients, suggesting protective roles. Based on the median NecroSig score, patients with PCOS were stratified into high- and low-risk groups (Fig. 3A). The high-risk group exhibited significantly lower live birth rates than the low-risk group (Fig. 3B). Among the six prognostic proteins, EIF2AK2 and ADAR showed significant expression differences between risk groups (Fig. 3C). Kaplan-Meier survival analysis confirmed that the low-risk group consistently demonstrated superior pregnancy outcomes (Fig. 3D).

3.6 Performance Validation and Clinical Relevance of the NecroSig Model

A nomogram integrating the six prognostic proteins was constructed to predict the probability of adverse pregnancy outcomes at 6 weeks (42 days), 28 weeks (196 days), and 37 weeks (259 days) (Fig. 4A). Time-dependent

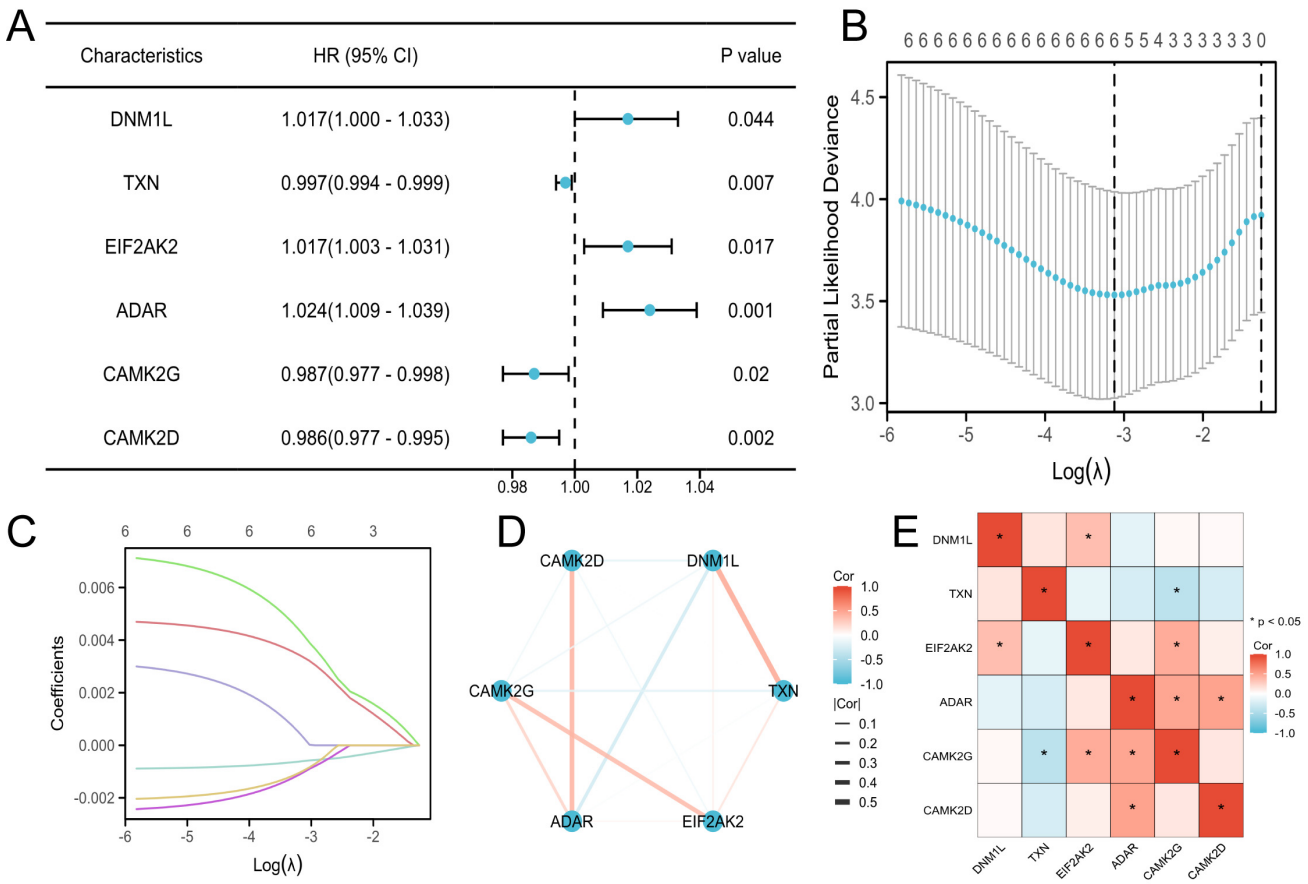

Fig. 2. Identification and analysis of prognostic necroptosis-related DEPs. (A) Forest plot of univariate Cox regression for necroptosis-related DEPs. (B) Partial likelihood deviance plot from LASSO regression. (C) LASSO coefficient profiles of the selected proteins. (D) PPI network of prognostic necroptosis-related proteins. (E) Correlation heatmap of the six necroptosis-related DEPs. DNM1L, dynamin 1 like; TXN, thioredoxin; EIF2AK2, eukaryotic translation initiation factor 2 alpha kinase 2; ADAR, adenosine deaminase acting on RNA; CAMK2D, calmodulin-dependent protein kinase II delta; CAMK2G, calmodulin-dependent protein kinase II gamma; LASSO, Least Absolute Shrinkage and Selection Operator; PPI, protein–protein interaction.

ROC analysis demonstrated strong predictive performance, with area under the curve (AUC) values of 0.828, 0.878, and 0.903 at 6, 28, and 37 weeks, respectively (Fig. 4B). At 37 weeks, the NecroSig model showed higher predictive accuracy than individual clinical parameters such as age (AUC = 0.551), BMI (0.712), AMH (0.592), insulin (0.684), HOMA-IR (0.673), TC (0.633), and TGs (0.633) (Fig. 4C1). A combined clinical model integrating these indicators yielded an AUC of 0.847, still lower than the NecroSig model (AUC = 0.903). When both proteomic and clinical indicators were integrated, the multimodal model demonstrated the highest predictive performance (AUC = 0.944) (Fig. 4C2). The multimodal model showed the highest discriminative ability, highlighting the complementary value of proteomic and clinical markers. DCA further confirmed that the NecroSig model provided greater net clinical benefit compared with conventional indicators (Fig. 4D). Heatmaps revealed distinct clinical feature distributions between high- and low-risk groups (Fig. 4E). Correlation analysis showed significant associations between EIF2AK2 and both fasting insulin and HOMA-IR, whereas TXN was negatively correlated with BMI (Fig. 4F).

3.7 Exploratory Correlation Analysis With Endometrial Receptivity Markers

Within the PCOS cohort, exploratory correlation analyses were conducted between the six necroptosis-related proteins and classical markers of endometrial receptivity, including homeobox A11 (HOXA11) and integrin subunit beta-1 (ITGB1), ITGB3, and ITGB5 [22]. Three significant associations were identified: DNM1L–ITGB1 (r = 0.38, p = 0.049), CAMK2G–ITGB3 (r = –0.41, p = 0.030), and CAMK2D–HOXA11 (r = –0.57, p = 0.013). These findings support a potential molecular crosstalk between necroptosis and integrin-mediated receptivity pathways (**Supplementary Fig. 1**; **Supplementary Tables 1,2**).

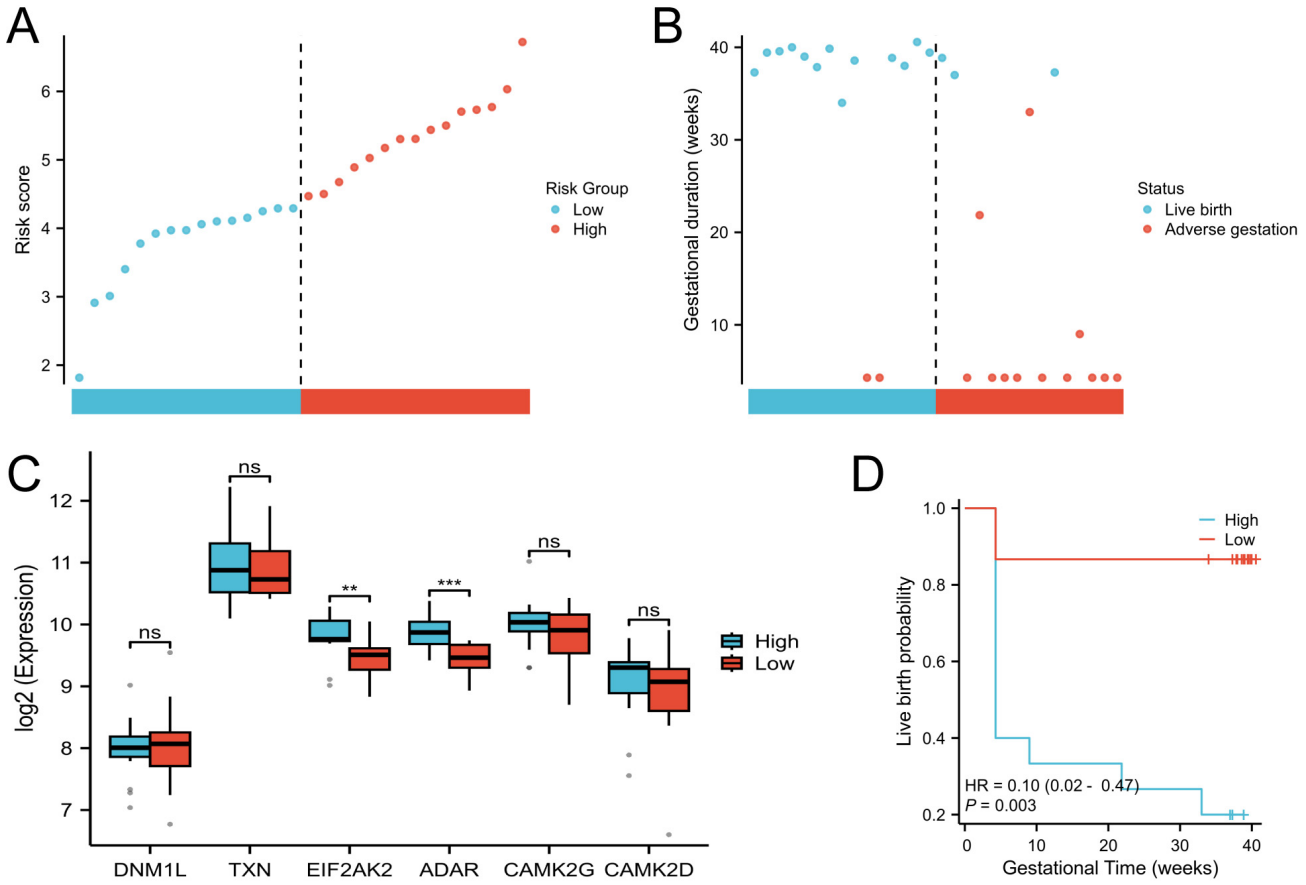

Fig. 3. Construction of the NecroSig model. (A) Distribution of risk scores. (B) Survival status plot showing the relationship between risk score and pregnancy outcome. (C) Boxplots of protein expression levels between risk groups. (D) Kaplan–Meier survival curves comparing pregnancy outcomes between high- and low-risk groups. ** $p < 0.01$; *** $p < 0.001$; ns, not significant.

4. Discussion

Impaired endometrial receptivity and ovulatory dysfunction are both central pathological features of infertility associated with PCOS, characterized by abnormal decidualization and failed embryo implantation, which increase the risk of adverse pregnancy outcomes such as miscarriage [5]. However, the mechanisms underlying endometrial dysfunction in PCOS remain incompletely understood, with multiple factors—including hormonal imbalances, IR, cytokine dysregulation, and chronic low-grade inflammation—potentially compromising endometrial receptivity [6]. In this study, quantitative proteomic analyses of the endometrium revealed that PCOS-associated differentially expressed proteins were significantly enriched in the necroptosis pathway, suggesting that necroptosis may play a key role in endometrial dysfunction and adverse pregnancy outcomes in patients with PCOS.

Necroptosis is a programmed cell death modality exhibiting features of both apoptosis and necrosis, whose excessive activation can trigger inflammatory responses and tissue damage [23,24]. We identified six key prognostic proteins (DNM1L, TXN, EIF2AK2, ADAR, CAMK2G, and CAMK2D). The mitochondrial fission protein DNM1L can drive excessive mitochondrial division, potentially inhibiting signal transducer and activator of transcription 1 phosphorylation and consequently affecting the expression of the endometrial receptivity marker HOXA10 [25–27]. Previous study has demonstrated that mitochondrial dysfunction in mice suppresses HOXA10 expression, impairs endometrial receptivity, and leads to embryo implantation failure [28]. Moreover, upregulation of ADAR in patients with PCOS reportedly mediates EIF2AK2 expression, possibly promoting PCOS progression via the mitogen-activated protein kinase pathway [29]. Consistently, our study identified ADAR and EIF2AK2 as risk factors for adverse pregnancy outcomes in PCOS, potentially through EIF2AK2-mediated overactivation of autophagy and subsequent activation of the NLR family pyrin domain containing 3 inflammasome, which negatively impacts endometrial receptivity [30–32]. Previous evidence also indicates that alterations in calcium homeostasis may contribute to implantation failure. An animal studyi has shown that CaMKII knockdown inhibits transcription factors nuclear factor of activated T-cells and nuclear factor kappa B, while reducing prostaglandin E2 (PGE2) and PGF2α secretion in mouse endometrial epithelial cells, potentially resulting in

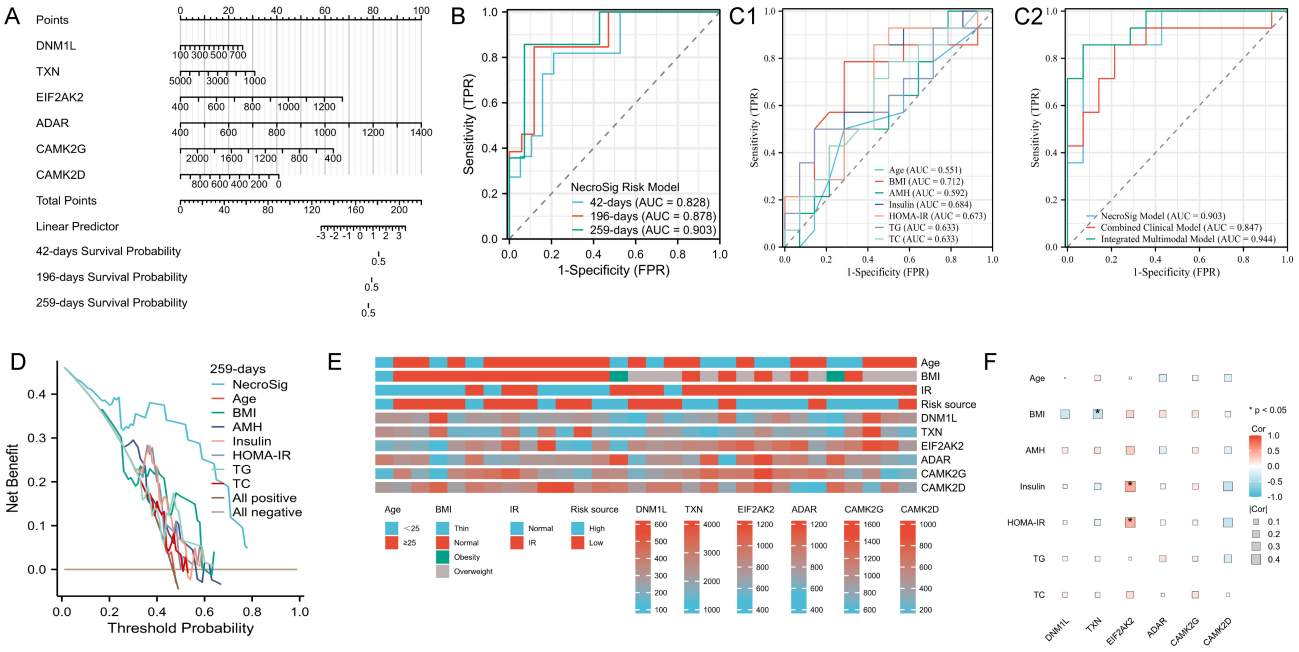

Fig. 4. Evaluation of model performance and correlation with clinical data. (A) Nomogram predicting adverse pregnancy risk at 6, 28, and 37 weeks. (B) Time-dependent ROC curves for live birth prediction. (C1) ROC curves of individual clinical indicators for predicting live birth at 37 weeks. (C2) Comparison between the NecroSig model, the combined clinical model, and the integrated multimodal model. (D) DCA for 37-week outcome prediction. (E) Heatmap showing distribution of clinical features across risk groups. (F) Correlation heatmap between clinical variables and prognostic proteins. AUC, area under the curve; TC, total cholesterol; TG, triglyceride; ROC, receiver operating characteristic; DCA, decision curve analysis; FPR, false positive rate; TPR, true positive rate.

implantation failure [33]. As a protective factor for pregnancy outcomes in PCOS, TXN promotes cell growth and proliferation, and its transcription level is elevated in decidualized endometrium [34].

Additionally, significant correlations observed among DNM1L–ITGB1, CAMK2G–ITGB3, and CAMK2D–HOXA11 further suggest potential regulatory links between necroptosis and endometrial receptivity, indicating that mitochondrial dynamics, calcium signaling, and cell adhesion pathways may cooperatively modulate implantation capacity in PCOS. Notably, integrating clinical indicators with the six-protein NecroSig signature improved the AUC from 0.903 to 0.944, suggesting that a multimodal model combining proteomic and metabolic–hormonal factors may provide more refined risk assessment in PCOS.

Integration of necroptosis-related proteins with clinical metabolic indices provides further insights into the metabolic dysregulation observed in patients with PCOS. EIF2AK2 (also known as PKP), a key mediator of inflammation, IR, and glucose homeostasis in obesity, was positively correlated with insulin levels and the HOMA-IR index, suggesting that EIF2AK2 may exacerbate endometrial metabolic dysfunction by interfering with insulin signaling [35,36]. IR can induce hyperandrogenism, thereby disrupting glucose metabolism and suppressing endometrial cell proliferation and activity, ultimately impairing endometrial receptivity [37]. Previous study has shown that TXN mitigates macrophage-driven inflammation in adipose tissue and reduces pro-inflammatory gut microbiota, alleviating high-fat diet-induced obesity and metabolic syndrome [38]. This finding supports our observation of a negative correlation between TXN expression and BMI, indicating that obesity-related oxidative stress may deplete protective proteins.

Beyond its mechanistic insights, the present study also holds potential clinical significance. The NecroSig model could serve as a valuable tool for stratifying patients with PCOS based on their predicted pregnancy risk, thereby supporting personalized clinical decision-making. For example, patients classified as high risk could benefit from individualized interventions such as insulin-sensitizing agents (e.g., metformin) or anti-inflammatory therapies aimed at restoring endometrial receptivity. Furthermore, integrating proteomic data with routinely available clinical biomarkers (e.g., AMH, HOMA-IR) may facilitate the development of simplified surrogate models suitable for clinical implementation. However, the high cost, technical complexity, and infrastructure requirements of LC–MS/MS-based proteomic profiling currently limit its use in routine reproductive medicine. Future efforts should focus on translating the proteomic signature into clinically measurable surrogates or immunoassay-based platforms, thereby improving accessibility and promoting real-world application of precision endometrial assessment in PCOS.

Despite the robust predictive performance of the NecroSig model constructed in this study, several limitations should be acknowledged. First, the single-center design and the relatively small sample size—particularly the limited number of control endometrial samples—may restrict the generalizability of our findings. The small control cohort also reduces statistical power for differential protein detection and increases sensitivity to individual variability or outliers, which may elevate the risk of false-positive identifications despite stringent FDR correction. This limitation mainly reflects the ethical and practical challenges of obtaining endometrial tissues from healthy fertile women. Although the control sample was limited, a post hoc power estimation (power ≈0.95) demonstrated that the study retained sufficient sensitivity for detecting large proteomic differences, supporting the reliability of our main findings. Moreover, given the limited cohort size, the LASSO–Cox–based NecroSig model should be regarded as exploratory, requiring external validation before clinical application. To address this limitation, future research will incorporate a multicenter validation design involving larger and demographically diverse cohorts, following harmonized inclusion and exclusion criteria across sites. Based on preliminary power estimations, approximately 150–200 patients with PCOS and 50–60 controls, matched for age and BMI, will be recruited for the study to enable cross-validation and model recalibration. Standardized protocols for endometrial sampling, protein quantification, and bioinformatics processing will be implemented to ensure methodological consistency and enhance external validity. Furthermore, the biological roles of the six NecroSig proteins were primarily deduced from bioinformatics and the literature, meaning that functional experiments remain necessary to confirm their exact mechanistic contribution to endometrial receptivity. Finally, the study did not dynamically track molecular changes in the endometrium across different menstrual cycles or following interventions. Future studies integrating multi-omics approaches and *in vitro* functional assays are warranted to further elucidate the molecular mechanisms of necroptosis in PCOS-related endometrial dysfunction and explore the feasibility of targeting these proteins for therapeutic intervention.

5. Conclusion

This study identified six necroptosis-related proteins associated with pregnancy outcomes in PCOS and developed a preliminary necroptosis-based prognostic framework (NecroSig). The model demonstrated promising predictive potential within this exploratory cohort, suggesting that necroptosis may be involved in the pathophysiology of PCOS through effects on endometrial receptivity and embryo implantation. These findings provide new insights into the molecular mechanisms underlying PCOS and offer a foundation for future studies aimed at validating and refining individualized risk prediction and therapeutic strategies.

Availability of Data and Materials

The mass spectrometry proteomics data generated in this study have been deposited in the ProteomeXchange Consortium via the iProX partner repository (http://proteomecentral.proteomexchange.org) under the dataset identifier PXD032383. Clinical data derived from patient records cannot be publicly released due to institutional privacy regulations and ethical restrictions. However, these data are available from the corresponding author upon reasonable request and with appropriate ethics approval, in accordance with institutional and national guidelines.

Author Contributions

KXW and FW jointly designed the study. WHX and XLT collected the data; WHX and CBT performed data analysis and wrote the statistical results section; XLT verified the data, generated the figures, and contributed to writing the results description. All authors contributed to editorial changes in the manuscript. All authors read and approved the final manuscript. All authors have participated sufficiently in the work and agreed to be accountable for all aspects of the work.

Ethics Approval and Consent to Participate

This study was approved by the Ethics Committee of the Second Hospital of Lanzhou University (Approval No. 2025A-774) for the secondary analysis of previously collected clinical and proteomic data. The original sample collection was conducted under a prior ethics approval by the Ethics Committee of the Second Hospital of Lanzhou University (Approval No. 2019A-057), and written informed consent had been obtained from all participants at the time of collection. All procedures were conducted in accordance with the ethical principles of the Declaration of Helsinki.

Acknowledgment

We thank Ejear for their professional manuscript editing service. All Figures in this study were created using Xiantao Academic (https://www.xiantaozi.com).

Funding

The research was supported by Cuiying Scientific and Technological Innovation Program of The Second Hospital & Clinical Medical School, Lanzhou University (Grant No. CY2023-MS-B13), Lanzhou Science and Technology Program Project (Grant No. 2023-ZD-82), the Natural Science Foundation of Gansu Province (Grant No. 24JRRA329) and the Natural Science Foundation of Gansu Province (Grant No. 22JR5RA974).

Conflict of Interest

The authors declare no conflict of interest.

Supplementary Material

Supplementary material associated with this article can be found, in the online version, at https://doi.org/10.31083/FBL47322.

References

[1] Joshi A. PCOS stratification for precision diagnostics and treatment. Frontiers in Cell and Developmental Biology. 2024; 12: 1358755. https://doi.org/10.3389/fcell.2024.1358755.

[2] Siddiqui S, Mateen S, Ahmad R, Moin S. A brief insight into the etiology, genetics, and immunology of polycystic ovarian syndrome (PCOS). Journal of Assisted Reproduction and Genetics. 2022; 39: 2439–2473. https://doi.org/10.1007/s10815-022-02625-7.

[3] Li Y, Fang Y, Wang H, Zhang H. Balancing Act: Exploring the Gut Microbiota-Brown Adipose Tissue Axis in PCOS Pathogenesis and Therapeutic Frontiers. Frontiers in Bioscience (Landmark edition). 2024; 29: 208. https://doi.org/10.31083/j.fbl2906208.

[4] Jiang NX, Li XL. The Disorders of Endometrial Receptivity in PCOS and Its Mechanisms. Reproductive Sciences (Thousand Oaks, Calif.). 2022; 29: 2465–2476. https://doi.org/10.1007/s43032-021-00629-9.

[5] Zhao J, Chen Q, Xue X. An Update on the Progress of Endometrial Receptivity in Women with Polycystic Ovary Syndrome. Reproductive Sciences (Thousand Oaks, Calif.). 2022; 29: 2136–2144. https://doi.org/10.1007/s43032-021-00641-z.

[6] Bai X, Zheng L, Li D, Xu Y. Research progress of endometrial receptivity in patients with polycystic ovary syndrome: a systematic review. Reproductive Biology and Endocrinology: RB&E. 2021; 19: 122. https://doi.org/10.1186/s12958-021-00802-4.

[7] Sayutti N, Abu MA, Ahmad MF. PCOS and Role of Cumulus Gene Expression in Assessing Oocytes Quality. Frontiers in Endocrinology. 2022; 13: 843867. https://doi.org/10.3389/fendo.2022.843867.

[8] Wang C, Wen YX, Mai QY. Impact of metabolic disorders on endometrial receptivity in patients with polycystic ovary syndrome. Experimental and Therapeutic Medicine. 2022; 23: 221. https://doi.org/10.3892/etm.2022.11145.

[9] Zhang J, Bao Y, Zhou X, Zheng L. Polycystic ovary syndrome and mitochondrial dysfunction. Reproductive Biology and Endocrinology: RB&E. 2019; 17: 67. https://doi.org/10.1186/s12958-019-0509-4.

[10] Yi Yang, Liu J, Xu W. Naringenin and morin reduces insulin resistance and endometrial hyperplasia in the rat model of polycystic ovarian syndrome through enhancement of inflammation and autophagic apoptosis. Acta Biochimica Polonica. 2022; 69: 91–100. https://doi.org/10.18388/abp.2020_5722.

[11] Lessey BA, Young SL. What exactly is endometrial receptivity? Fertility and Sterility. 2019; 111: 611–617. https://doi.org/10.1016/j.fertnstert.2019.02.009.

[12] Weindel CG, Martinez EL, Zhao X, Mabry CJ, Bell SL, Vail KJ, *et al*. Mitochondrial ROS promotes susceptibility to infection via gasdermin D-mediated necroptosis. Cell. 2022; 185: 3214–3231.e23. https://doi.org/10.1016/j.cell.2022.06.038.

[13] Cao L, Gao S, Liu J, Wang J, Qin R. Selenomethionine protects against Escherichia coli-induced endometritis by inhibiting inflammation and necroptosis via regulating the PPAR-γ/NF-κB pathway. Chemico-biological Interactions. 2023; 379: 110532. https://doi.org/10.1016/j.cbi.2023.110532.

[14] Liang QQ, Shi ZJ, Yuan T, Chen SY, Li YP, Zhang HR, *et al*. Celastrol inhibits necroptosis by attenuating the RIPK1/RIPK3/MLKL pathway and confers protection against acute pancreatitis in mice. International Immunopharmacology. 2023; 117: 109974. https://doi.org/10.1016/j.intimp.2023.109974.

[15] Wang M, An K, Huang J, Mprah R, Ding H. A novel model based on necroptosis to assess progression for polycystic ovary syndrome and identification of potential therapeutic drugs. Frontiers in Endocrinology. 2023; 14: 1193992. https://doi.org/10.3389/fendo.2023.1193992.

[16] Yi Y, Gao K, Lin P, Chen H, Zhou D, Tang K, *et al*. *Staphylococcus aureus*-Induced Necroptosis Promotes Mitochondrial Damage in Goat Endometrial Epithelial Cells. Animals: an Open Access Journal from MDPI. 2022; 12: 2218. https://doi.org/10.3390/ani12172218.

[17] He L, Zheng S, Zhan F, Lin N. The role of necroptosis in pathological pregnancies: Mechanisms and therapeutic opportunities. Journal of Reproductive Immunology. 2025; 169: 104460. https://doi.org/10.1016/j.jri.2025.104460.

[18] Timur HT, Cimrin D, Gursoy Doruk O, Dogan OE. Determining the age group-based cut-off values of serum anti-Mullerian hormone concentrations to diagnose polycystic ovary syndrome. Current Medical Research and Opinion. 2023; 39: 855–863. https://doi.org/10.1080/03007995.2023.2204768.

[19] Li YL, Yan EQ, Zhao GN, Jin L, Ma BX. Effect of body mass index on ovarian reserve and ART outcomes in infertile women: a large retrospective study. Journal of Ovarian Research. 2024; 17: 195. https://doi.org/10.1186/s13048-024-01521-1.

[20] Bian L, Zhou Y, Zhang D, Jiang T, Xing C, Wu X, *et al*. Negative correlation between serum pyruvate kinase M2 and cognitive function in patients with cerebral small vessel disease. Clinical Neurology and Neurosurgery. 2023; 225: 107586. https://doi.org/10.1016/j.clineuro.2023.107586.

[21] Chen Y, Chen J, Li Y, Wu Y, Wu X, Zhang H, *et al*. Insulin-like peptide 5 is associated with insulin resistance in women with polycystic ovary syndrome. Journal of Diabetes and its Complications. 2023; 37: 108493. https://doi.org/10.1016/j.jdiacomp.2023.108493.

[22] Zhang X, Gong S, Li H, Jiang J, Jia Y, Zhang R, *et al*. USP18 promotes endometrial receptivity via the JAK/STAT1 and the ISGylation pathway. Theriogenology. 2023; 202: 110–118. https://doi.org/10.1016/j.theriogenology.2023.03.011.

[23] Zhou Y, Cai Z, Zhai Y, Yu J, He Q, He Y, *et al*. Necroptosis inhibitors: mechanisms of action and therapeutic potential. Apoptosis: an International Journal on Programmed Cell Death. 2024; 29: 22–44. https://doi.org/10.1007/s10495-023-01905-6.

[24] Kang K, Park C, Chan FKM. Necroptosis at a glance. Journal of Cell Science. 2022; 135: jcs260091. https://doi.org/10.1242/jcs.260091.

[25] Wang X, Chen Z, Fan X, Li W, Qu J, Dong C, *et al*. Inhibition of DNM1L and mitochondrial fission attenuates inflammatory response in fibroblast-like synoviocytes of rheumatoid arthritis. Journal of Cellular and Molecular Medicine. 2020; 24: 1516–1528. https://doi.org/10.1111/jcmm.14837.

[26] Zhang J, Xie W, Ni B, Li Z, Feng D, Zhang Y, *et al*. NSD2 modulates Drp1-mediated mitochondrial fission in chronic renal allograft interstitial fibrosis by methylating STAT1. Pharmacological Research. 2024; 200: 107051. https://doi.org/10.1016/j.phrs.2023.107051.

[27] Fan X, Wei J, Guo Y, Ma J, Qi M, Huang H, *et al*. LPS Disrupts Endometrial Receptivity by Inhibiting STAT1 Phosphorylation in Sheep. International Journal of Molecular Sciences. 2024; 25: 13673. https://doi.org/10.3390/ijms252413673.

[28] Ren R, Zhou X, Jia T, Wang B, Liu A, Gao M, *et al*. Developmental exposure to perfluorooctane sulfonate(PFOS) impairs the endometrial receptivity. Scientific Reports. 2025; 15: 1747. https://doi.org/10.1038/s41598-024-84732-2.

[29] Kong FS, Feng J, Yao JP, Lu Y, Guo T, Sun M, *et al*. Dysregulated RNA editing of EIF2AK2 in polycystic ovary syndrome:

clinical relevance and functional implications. BMC Medicine. 2024; 22: 229. https://doi.org/10.1186/s12916-024-03434-8.

[30] Balci CN, Acar N. NLRP3 inflammasome pathway, the hidden balance in pregnancy: A comprehensive review. Journal of Reproductive Immunology. 2024; 161: 104173. https://doi.org/10.1016/j.jri.2023.104173.

[31] Cao Z, Wang Y, Long Z, He G. Interaction between autophagy and the NLRP3 inflammasome. Acta Biochimica et Biophysica Sinica. 2019; 51: 1087–1095. https://doi.org/10.1093/abbs/gmz098.

[32] Niso-Santano M, Shen S, Adjemian S, Malik SA, Mariño G, Lachkar S, *et al*. Direct interaction between STAT3 and EIF2AK2 controls fatty acid-induced autophagy. Autophagy. 2013; 9: 415–417. https://doi.org/10.4161/auto.22910.

[33] Shukla V, Kaushal JB, Kumar R, Popli P, Agnihotri PK, Mitra K, *et al*. Microtubule depolymerization attenuates WNT4/CaMKIIα signaling in mouse uterus and leads to implantation failure. Reproduction (Cambridge, England). 2019; 158: 47–59. https://doi.org/10.1530/REP-18-0611.

[34] Simmons DG, Kennedy TG. Rat endometrial Vdup1 expression: changes related to sensitization for the decidual cell reaction and hormonal control. Reproduction (Cambridge, England). 2004; 127: 475–482. https://doi.org/10.1530/rep.1.00029.

[35] Udumula MP, Babu MS, Bhat A, Dhar I, Sriram D, Dhar A. High glucose impairs insulin signaling via activation of PKR pathway in L6 muscle cells. Biochemical and Biophysical Research Communications. 2017; 486: 645–651. https://doi.org/10.1016/j.bbrc.2017.03.078.

[36] Yalçin A, Şarkici G, Kolaç UK. PKR inhibitors suppress endoplasmic reticulum stress and subdue glucolipotoxicity-mediated impairment of insulin secretion in pancreatic beta cells. Turkish Journal of Biology = Turk Biyoloji Dergisi. 2020; 44: 93–102. https://doi.org/10.3906/biy-1909-20.

[37] He FF, Li YM. Role of gut microbiota in the development of insulin resistance and the mechanism underlying polycystic ovary syndrome: a review. Journal of Ovarian Research. 2020; 13: 73. https://doi.org/10.1186/s13048-020-00670-3.

[38] Newman NK, Zhang Y, Padiadpu J, Miranda CL, Magana AA, Wong CP, *et al*. Reducing gut microbiome-driven adipose tissue inflammation alleviates metabolic syndrome. Microbiome. 2023; 11: 208. https://doi.org/10.1186/s40168-023-01637-4.